Preliminary Assessment of a Bayesian Compressive Sampling-based Contrast Field Inversion Method

L. Poli, G. Oliveri, A. Massa

Abstract

In this report, the effectiveness of a novel strategy exploiting the Compressive Sensing paradigm for imaging sparse scatterers at microwave frequencies has been preliminary investigated. After a suitable calibration procedure of the proposed strategy, some introductory results about sparse and weak scatterers have been presented.

Contents

1 TEST CASE: Calibration

Goal: show the performances of BCS when dealing with a sparse scatterer

- Number of Views: V
- Number of Measurements: M
- Number of Cells for the Inversion: N
- Number of Cells for the Direct solver: D
- Side of the investigation domain: L

Test Case Description

Direct solver:

- Square domain divided in $\sqrt{D} \times \sqrt{D}$ cells
- Domain side: $L = 3\lambda$
- $D = 1296$ (discretization for the direct solver: $< \lambda/10$)

Investigation domain:

- Square domain divided in $\sqrt{N} \times \sqrt{N}$ cells
- $L = 3\lambda$
- $2ka = 2 \times \frac{2\pi}{\lambda} \times \frac{L\sqrt{2}}{2} = 6\pi\sqrt{2} = 26.65$
- $\#DOF = \frac{(2ka)^2}{2} = \frac{(2\times\frac{2\pi}{\lambda}\times\frac{L\sqrt{2}}{2})^2}{2} = 4\pi^2\left(\frac{L}{\lambda}\right)^2 = 4\pi^2 \times 9 \approx 355.3$
- N scelto in modo da essere vicino a $\#DOF$: $N = 324$ (18×18)

Measurement domain:

- Measurement points taken on a circle of radius $\rho = 3\lambda$
- Full-aspect measurements
- $M \approx 2ka \rightarrow M = 27$

Sources:

- Plane waves
- $V \approx 2ka \rightarrow V = 27$
- Amplitude $A = 1$
- Frequency: 300 MHz $(\lambda = 1)$

Object:

- Square cylinder of side $\frac{\lambda}{6} = 0.1667$
- Low ε_r values: $\varepsilon_r \in \{1.5, 2.0, 2.5, 3.0\}$
- Very Low ε_r values: $\varepsilon_r \in \{1.1, 1.2, 1.3, 1.4\, 1.5\}$

- $\sigma = 0$ [S/m]

BCS parameters:

- Initial estimate of the noise: $n_0^2 \in \{1.0 \times 10^{-6}, 2.0 \times 10^{-6}, 5.0 \times 10^{-6}, 1.0 \times 10^{-5}, 2.0 \times 10^{-5}, 5.0 \times 10^{-5}, 1.0 \times 10^{-4}, 2.0 \times 10^{-4}, 5.0 \times 10^{-4}, 1.0 \times 10^{-3}, 2.0 \times 10^{-3}, 5.0 \times 10^{-2}, 1.0 \times 10^{-2}, 2.0 \times 10^{-2}, 5.0 \times 10^{-2}, \}$
- Convergenze parameter: $\tau = 10^{-8}$

1.1 Low ε_r Values - Noiseless case

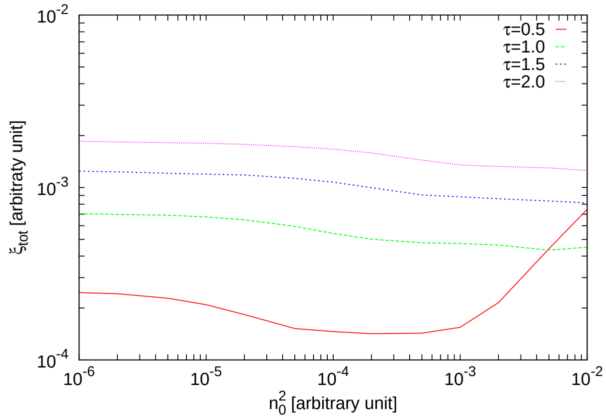

(a)

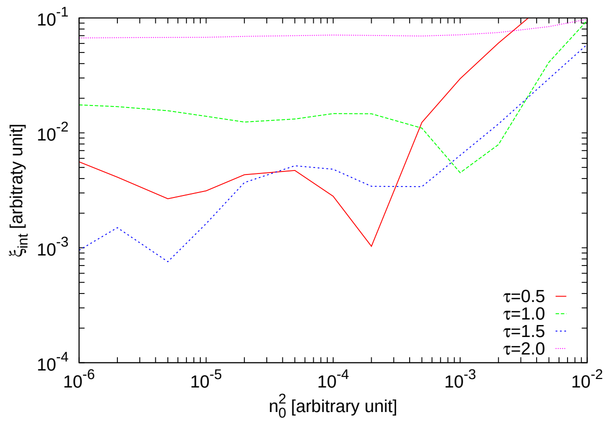

(b)

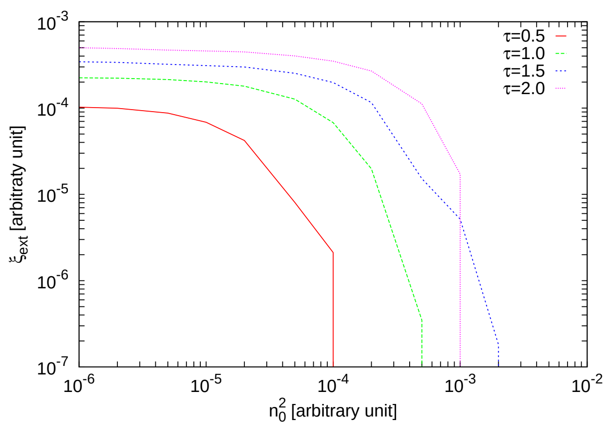

(c)

Figure 139. *Calibration* (Noiseless case) - Behaviour of error figures as a function of n_0^2 and τ: (a) total error ξ_{tot}, (b) internal error ξ_{int}, (c) external error ξ_{ext}.

1.2 Low ε_r Values - $SNR = 20$ [dB]

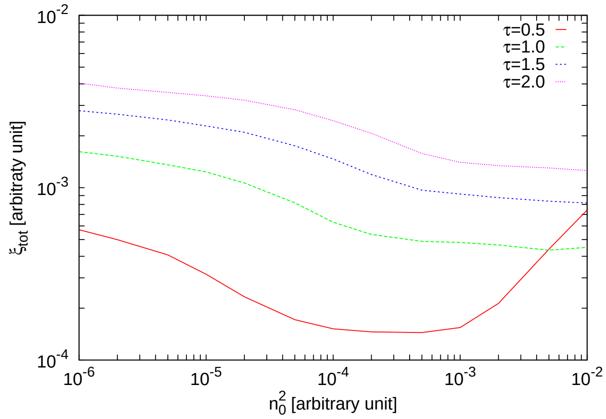

(a)

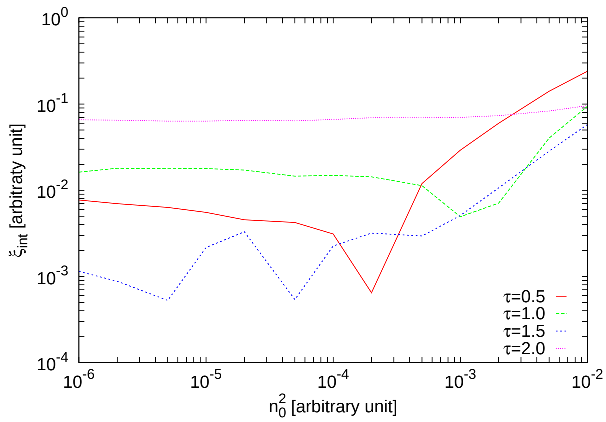

(b)

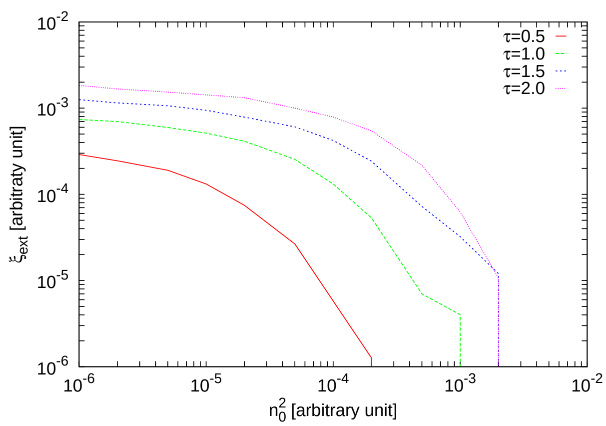

(c)

Figure 140. *Calibration* ($SNR = 20$ [dB]) - Behaviour of error figures as a function of n_0^2 and τ: (a) total error ξ_{tot}, (b) internal error ξ_{int}, (c) external error ξ_{ext}.

1.3 Low ε_r Values - $SNR = 10$ [dB]

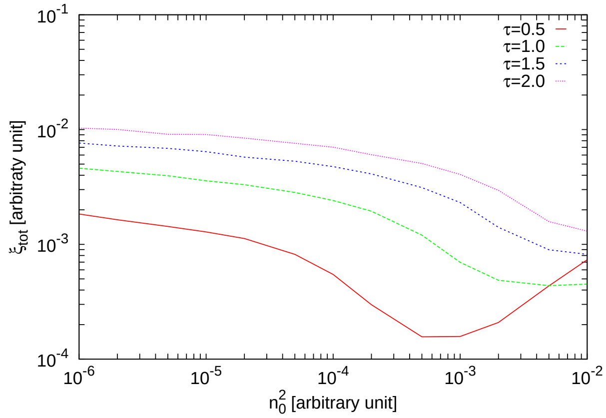

(a)

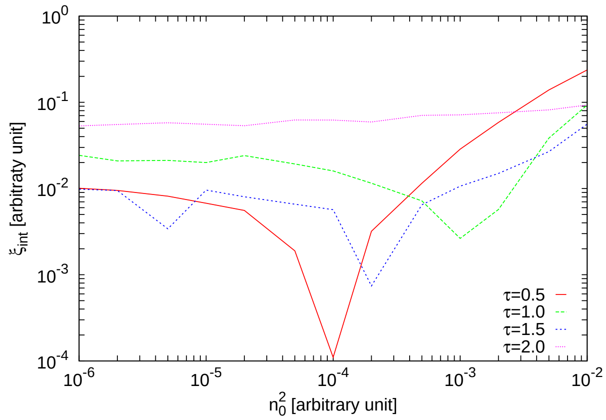

(b)

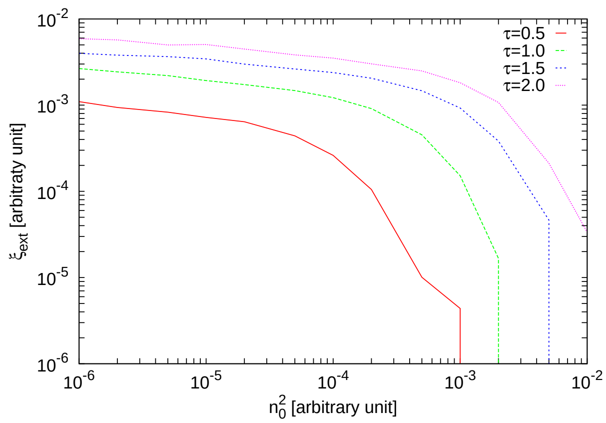

(c)

Figure 141. *Calibration* ($SNR = 10$ [dB]) - Behaviour of error figures as a function of n_0^2 and τ: (a) total error ξ_{tot}, (b) internal error ξ_{int}, (c) external error ξ_{ext}.

1.4 Low ε_r Values - $SNR = 5$ [dB]

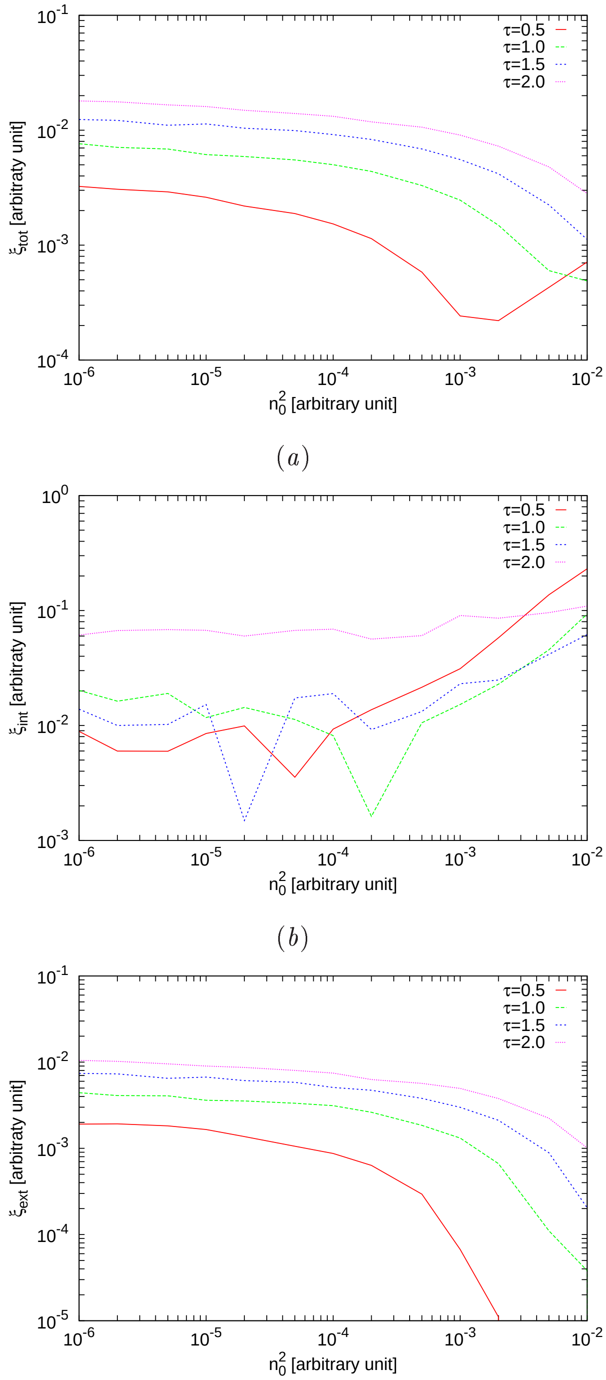

(a)

(b)

(c)

Figure 142. *Calibration* ($SNR = 5$ [dB]) - Behaviour of error figures as a function of n_0^2 and τ: (a) total error ξ_{tot}, (b) internal error ξ_{int}, (c) external error ξ_{ext}.

1.5 Very Low ε_r Values - Noiseless case

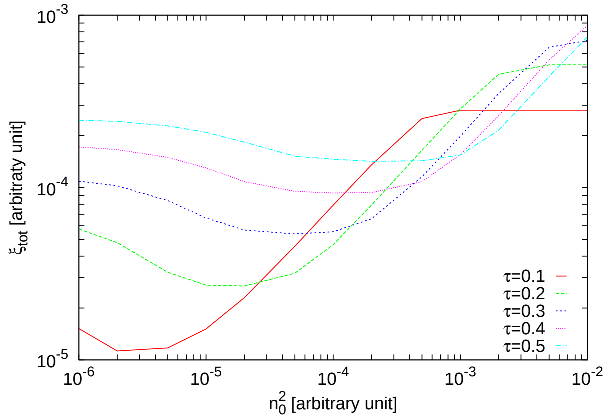

(a)

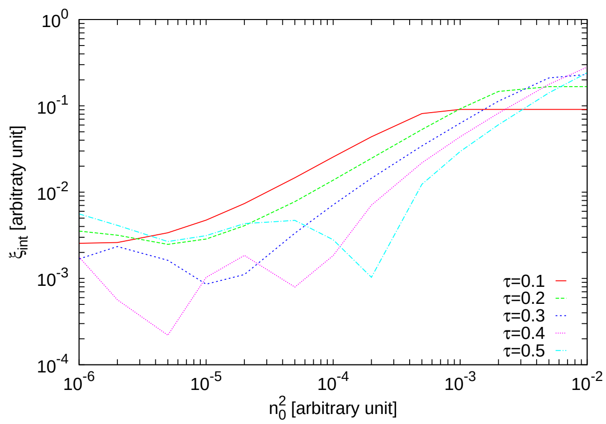

(b)

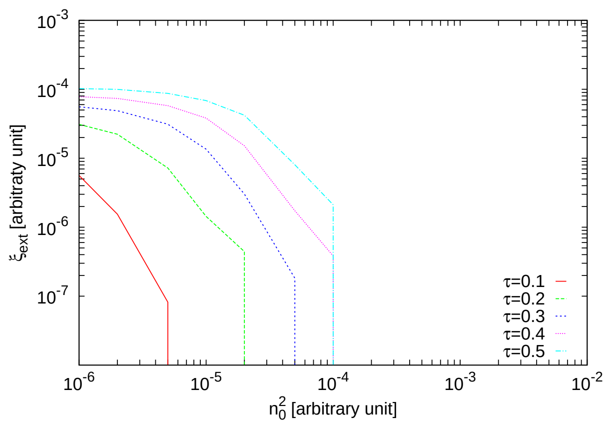

(c)

Figure 143. *Calibration* (Noiseless case) - Behaviour of error figures as a function of n_0^2 and τ: (a) total error ξ_{tot}, (b) internal error ξ_{int}, (c) external error ξ_{ext}.

1.6 Very Low ε_r Values - $SNR = 20$ [dB]

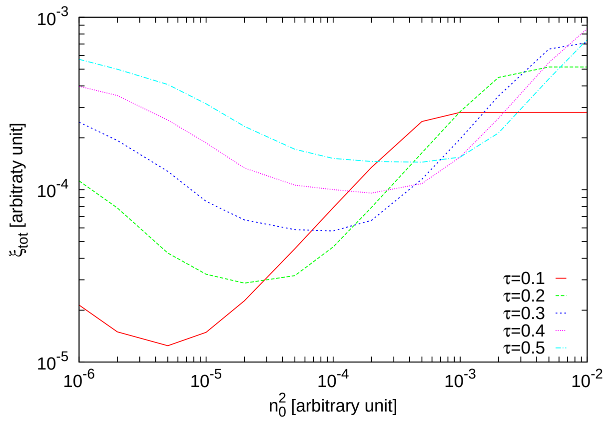

(a)

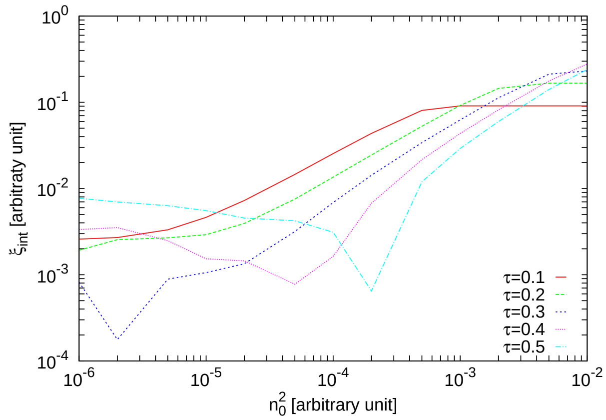

(b)

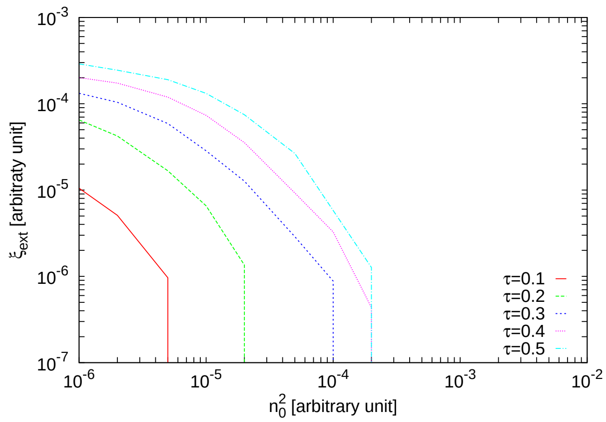

(c)

Figure 144. *Calibration* ($SNR = 20$ [dB]) - Behaviour of error figures as a function of n_0^2 and τ: (a) total error ξ_{tot}, (b) internal error ξ_{int}, (c) external error ξ_{ext}.

1.7 Very Low ε_r Values - $SNR = 10$ [dB]

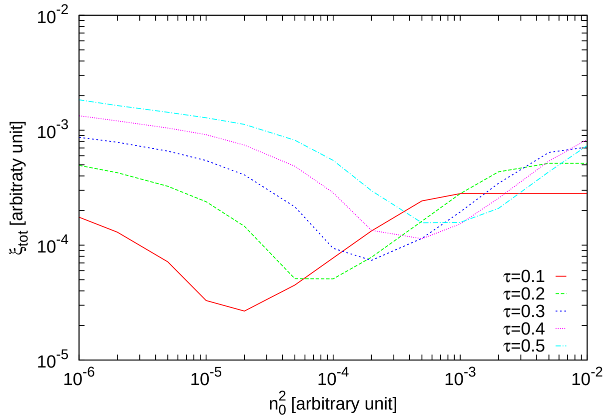

(a)

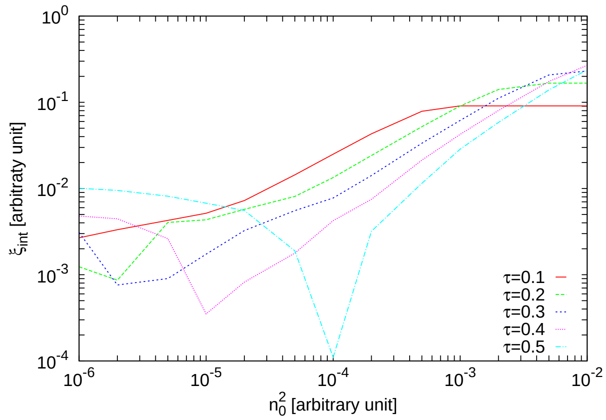

(b)

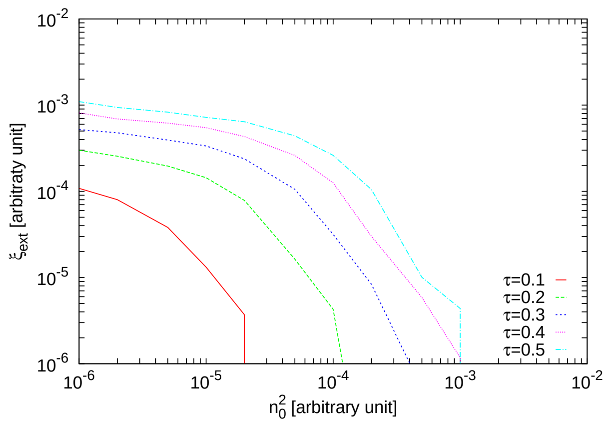

(c)

Figure 145. *Calibration* ($SNR = 10$ [dB]) - Behaviour of error figures as a function of n_0^2 and τ: (a) total error ξ_{tot}, (b) internal error ξ_{int}, (c) external error ξ_{ext}.

1.8 Very Low ε_r Values - $SNR = 5$ [dB]

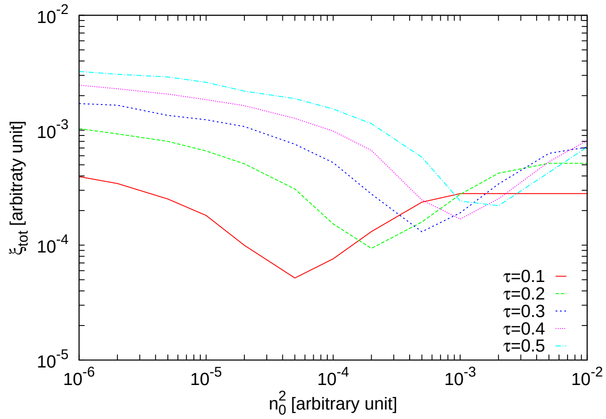

(a)

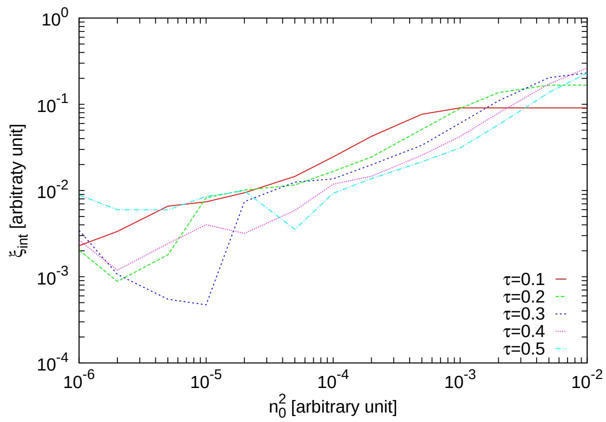

(b)

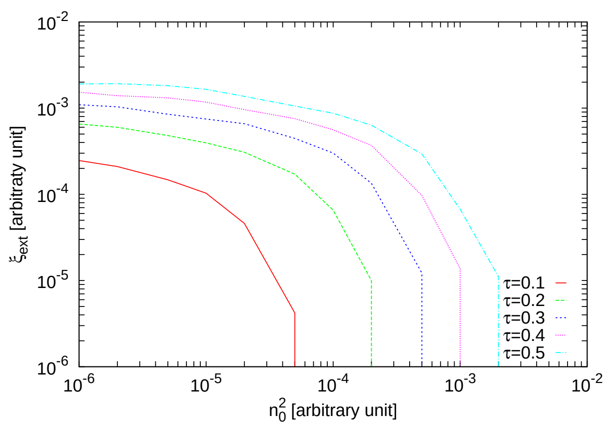

(c)

Figure 146. *Calibration* ($SNR = 5$ [dB]) - Behaviour of error figures as a function of n_0^2 and τ: (a) total error ξ_{tot}, (b) internal error ξ_{int}, (c) external error ξ_{ext}.

2 TEST CASE: Square Cylinder $l = 0.16\lambda$

Goal: show the performances of BCS when dealing with a sparse scatterer

- Number of Views: V
- Number of Measurements: M
- Number of Cells for the Inversion: N
- Number of Cells for the Direct solver: D
- Side of the investigation domain: L

Test Case Description

Direct solver:

- Square domain divided in $\sqrt{D} \times \sqrt{D}$ cells
- Domain side: $L = 3\lambda$
- $D = 1296$ (discretization for the direct solver: $< \lambda/10$)

Investigation domain:

- Square domain divided in $\sqrt{N} \times \sqrt{N}$ cells
- $L = 3\lambda$
- $2ka = 2 \times \frac{2\pi}{\lambda} \times \frac{L\sqrt{2}}{2} = 6\pi\sqrt{2} = 26.65$
- $\#DOF = \frac{(2ka)^2}{2} = \frac{(2\times\frac{2\pi}{\lambda}\times\frac{L\sqrt{2}}{2})^2}{2} = 4\pi^2\left(\frac{L}{\lambda}\right)^2 = 4\pi^2 \times 9 \approx 355.3$
- N scelto in modo da essere vicino a $\#DOF$: $N = 324$ (18×18)

Measurement domain:

- Measurement points taken on a circle of radius $\rho = 3\lambda$
- Full-aspect measurements
- $M \approx 2ka \rightarrow M = 27$

Sources:

- Plane waves
- $V \approx 2ka \rightarrow V = 27$
- Amplitude $A = 1$
- Frequency: 300 MHz $(\lambda = 1)$

Object:

- Square cylinder of side $\frac{\lambda}{6} = 0.1667$
- $\varepsilon_r \in \{1.5, 2.0, 2.5, 3.0\}$
- $\sigma = 0$ [S/m]

BCS parameters:

- Initial estimate of the noise: $n_0 = 1.0 \times 10^{-3}$
- Convergenze parameter: $\tau = 1.0 \times 10^{-8}$

RESULTS: $\varepsilon_r = 1.5$

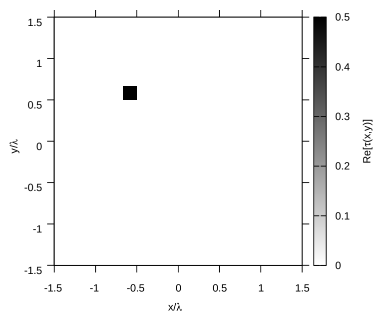

(a)

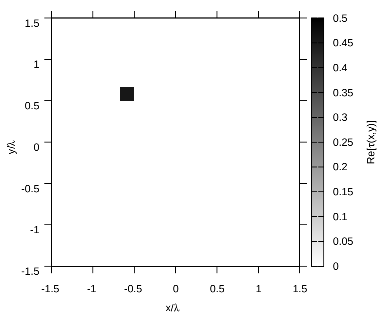

(b)

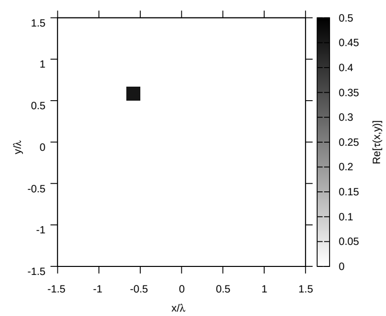

(c)

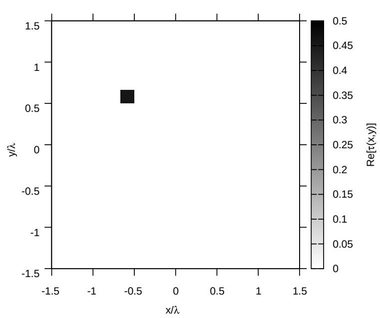

(d)

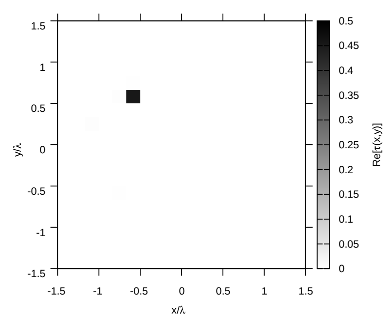

(e)

Figure 1. Actual object (a) and BCS reconstructed object for (b) Noiseless case, (c) $SNR = 20$ [dB] , (d) $SNR = 10$ [dB] , (e) $SNR = 5$ [dB].

RESULTS: $\varepsilon_r = 2.0$

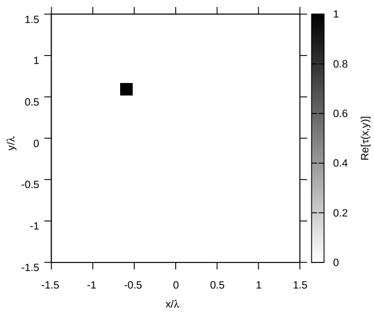

(a)

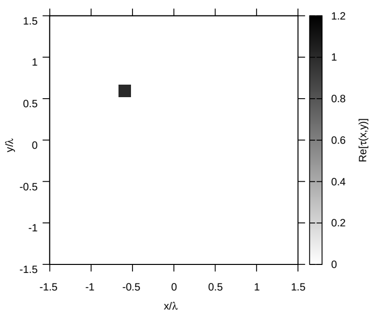

(b)

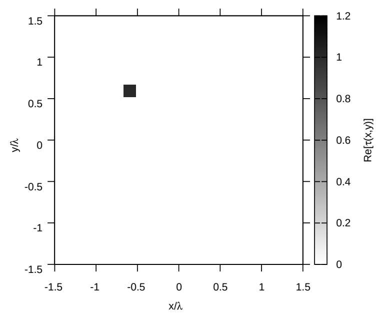

(c)

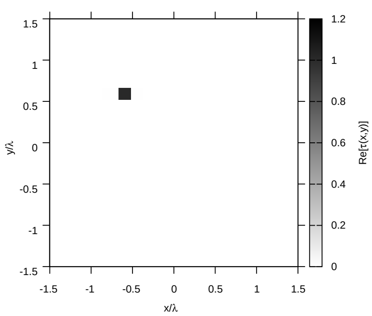

(d)

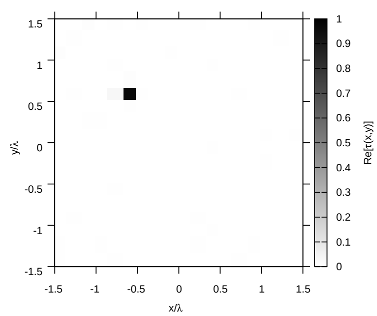

(e)

Figure 2. Actual object (a) and BCS reconstructed object for (b) Noiseless case, (c) $SNR = 20$ [dB] , (d) $SNR = 10$ [dB] , (e) $SNR = 5$ [dB].

RESULTS: $\varepsilon_r = 2.5$

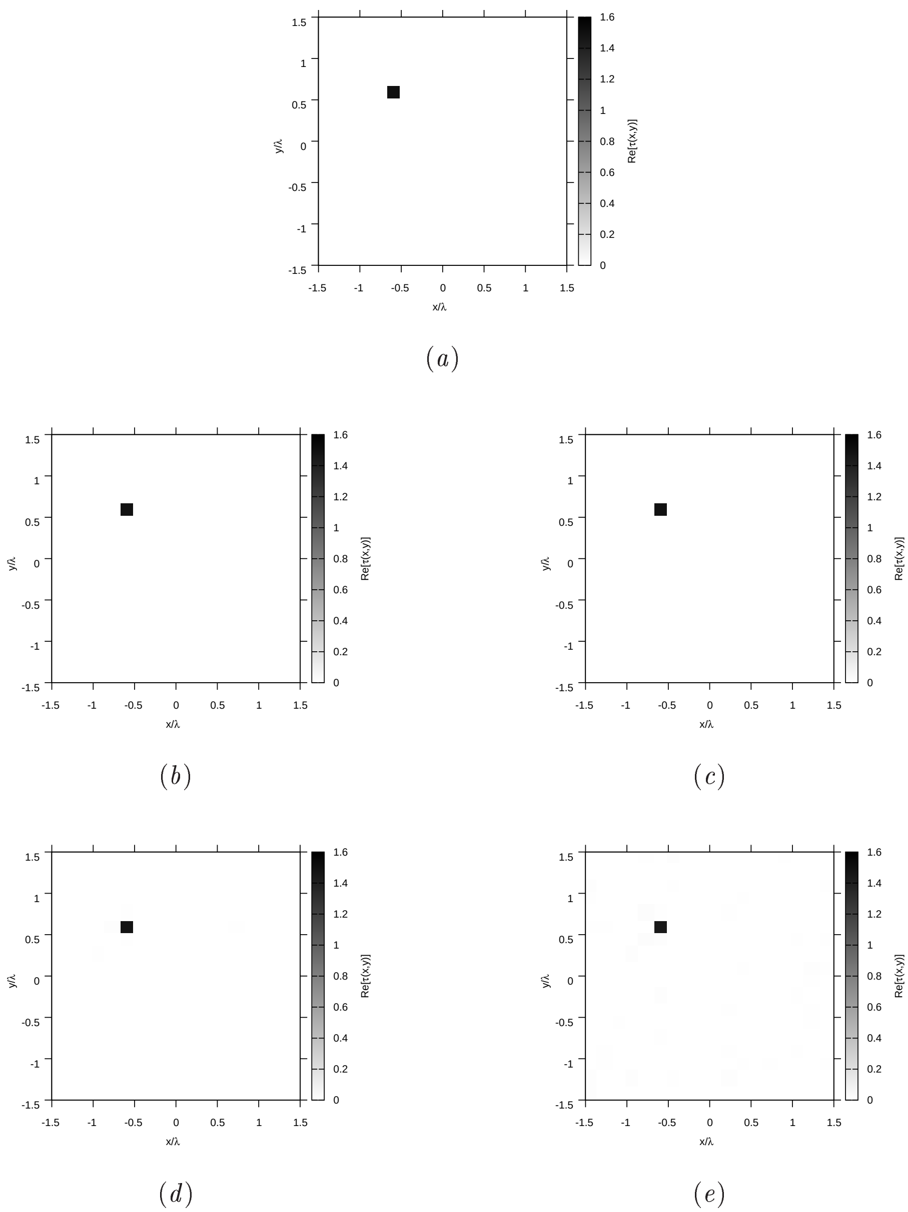

Figure 3. Actual object (a) and BCS reconstructed object for (b) Noiseless case, (c) $SNR = 20$ [dB] , (d) $SNR = 10$ [dB] , (e) $SNR = 5$ [dB].

RESULTS: $\varepsilon_r = 3.0$

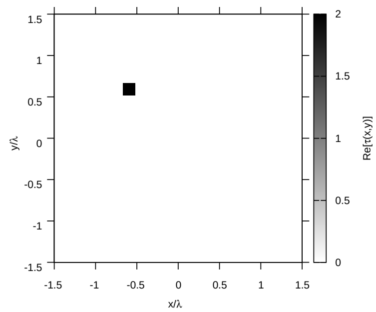

(a)

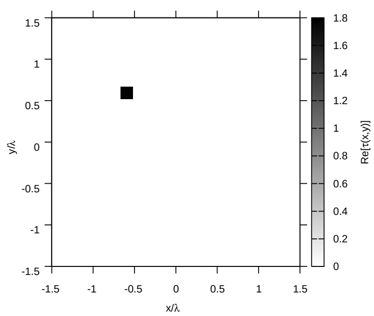

(b)

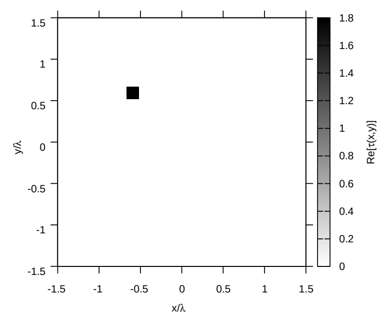

(c)

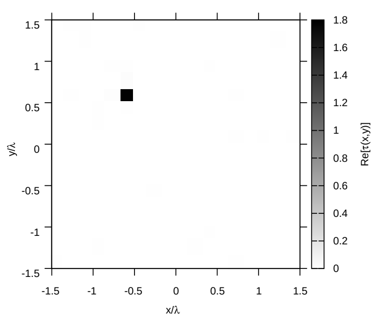

(d)

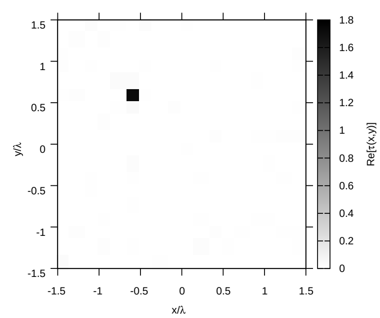

(e)

Figure 4. Actual object (a) and BCS reconstructed object for (b) Noiseless case, (c) $SNR = 20$ [dB] , (d) $SNR = 10$ [dB] , (e) $SNR = 5$ [dB].

Observations:

Ricostruzioni molto buone per tutti i valori di SNR, fino a $\varepsilon_r = 3.0$.

RESULTS: Error Figures

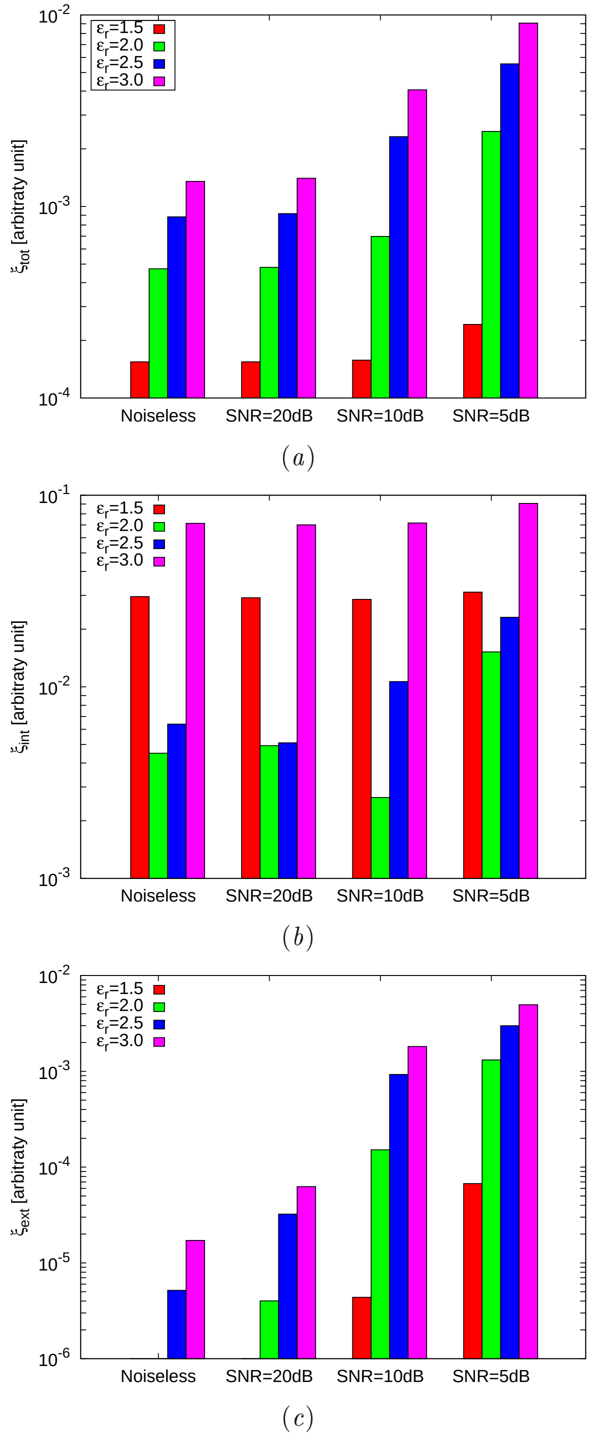

Figure 5. Behaviour of error figures as a function of ε_r, for different SNR values: (a) total error ξ_{tot}, (b) internal error ξ_{int}, (c) external error ξ_{ext}.

Observations:

La condizione di validità riportata in [5], ci consente di ricavare il valore di ε_r massimo tale per cui è possibile applicare l'approssimazione di Born per il caso in questione, con oggetto scatteratore di dimensione pari a $\frac{\lambda}{6}$:

$$n_\delta a < \frac{\lambda}{4}$$

dove a è il raggio dell'oggetto e $n_\delta = \sqrt{\frac{\mu\varepsilon}{\mu_0\varepsilon_0}}$.
Ne caso in questione otteniamo quindi: $\sqrt{\varepsilon_r} < \frac{\lambda}{4a} \;\Rightarrow\; \sqrt{\varepsilon_r} < \frac{12\lambda}{4\lambda} \;\Rightarrow\; \varepsilon_r < 9$.

RESULTS: Error Figures

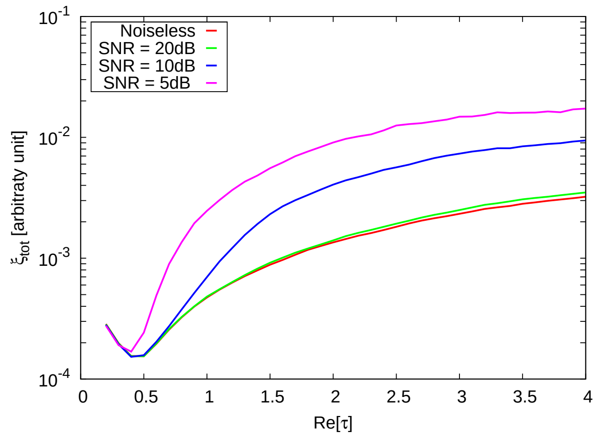

(a)

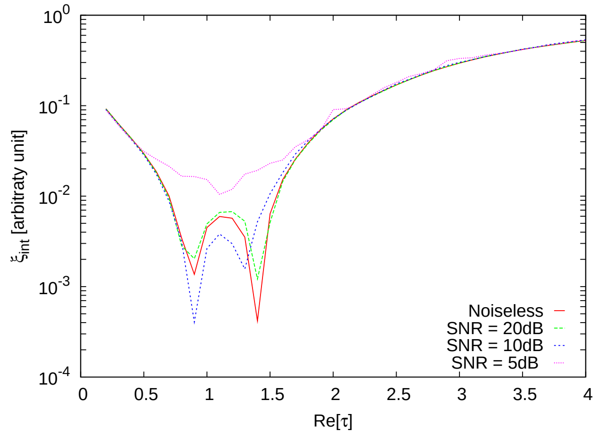

(b)

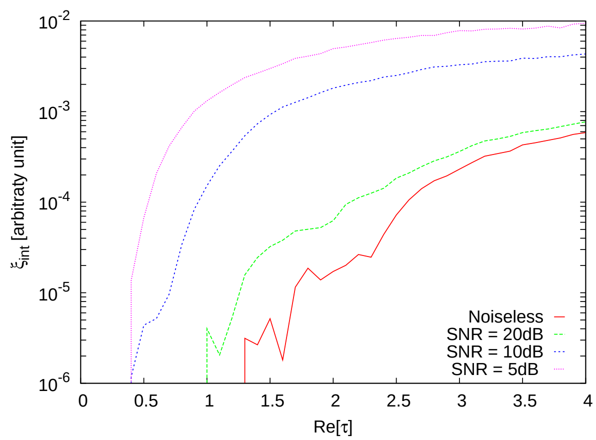

(c)

Figure 6. Behaviour of error figures as a function of ε_r, for different SNR values: (a) total error ξ_{tot}, (b) internal error ξ_{int}, (c) external error ξ_{ext}.

Observations:

L'errore interno sale vertiginosamente per valori di ε_r superiori a 2.5; in generale però, come si può osservare dalle figure delle ricostruzioni, le prestazioni sono buone fino a $\varepsilon_r = 3.0$.

Internal Scattered Field Analysis

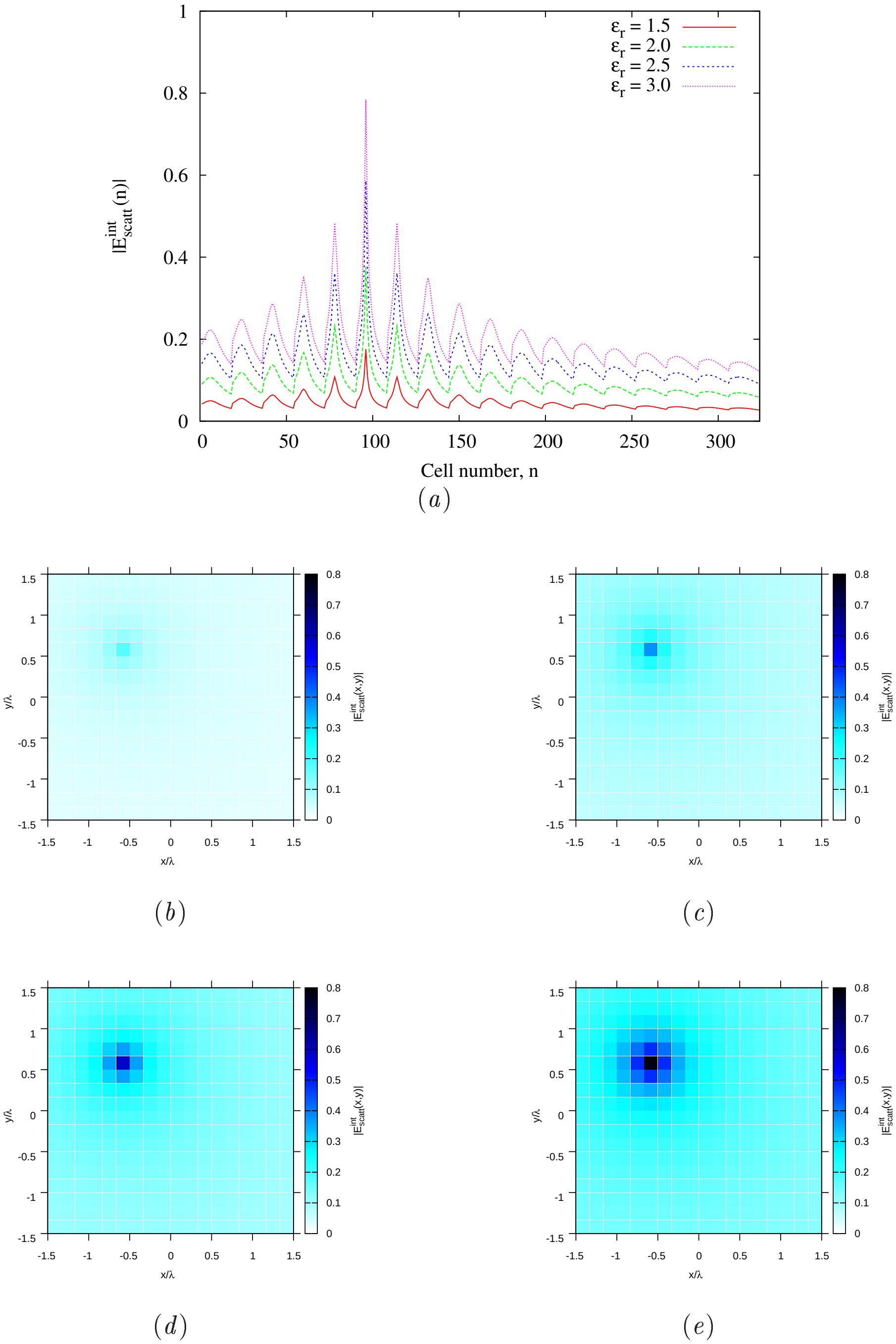

Figure 7.(a) Average of the absolute value of the scattered field inside the investigation domain for different values of ε_r : (b) $\varepsilon_r = 1.5$, (c) $\varepsilon_r = 2.0$, (d) $\varepsilon_r = 2.5$ and (e) $\varepsilon_r = 3.0$.

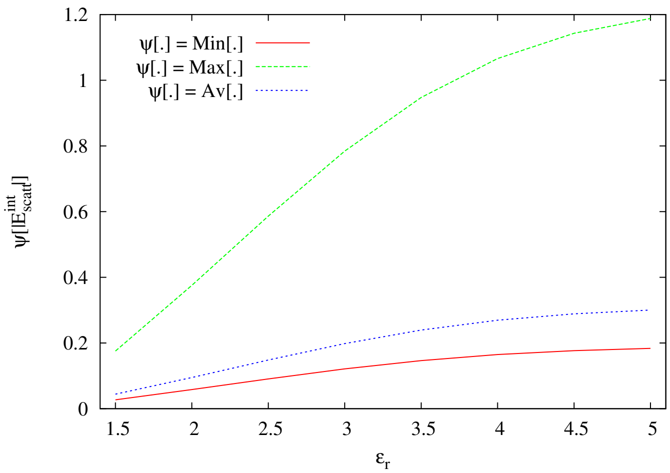

(a)

Figure 8.(a) Internal Scattered Field statistical analysis.

Observations:

Le prestazioni della tecnica si possono considerare buone fino a $\varepsilon_r = 3.0$, ossia, osservando Fig.8.(a), fino a quando $\frac{E^{int}_{tot} - E^{int}_{inc}}{E^{int}_{inc}} < 0.2$.

3 TEST CASE: Square Cylinder $side = 0.33\lambda$

Goal: show the performances of BCS when dealing with a sparse scatterer

- Number of Views: V
- Number of Measurements: M
- Number of Cells for the Inversion: N
- Number of Cells for the Direct solver: D
- Side of the investigation domain: L

Test Case Description

Direct solver:

- Square domain divided in $\sqrt{D} \times \sqrt{D}$ cells
- Domain side: $L = 3\lambda$
- $D = 1296$ (discretization for the direct solver: $< \lambda/10$)

Investigation domain:

- Square domain divided in $\sqrt{N} \times \sqrt{N}$ cells
- $L = 3\lambda$
- $2ka = 2 \times \frac{2\pi}{\lambda} \times \frac{L\sqrt{2}}{2} = 6\pi\sqrt{2} = 26.65$
- $\#DOF = \frac{(2ka)^2}{2} = \frac{(2\times\frac{2\pi}{\lambda}\times\frac{L\sqrt{2}}{2})^2}{2} = 4\pi^2\left(\frac{L}{\lambda}\right)^2 = 4\pi^2 \times 9 \approx 355.3$
- N scelto in modo da essere vicino a $\#DOF$: $N = 324$ (18×18)

Measurement domain:

- Measurement points taken on a circle of radius $\rho = 3\lambda$
- Full-aspect measurements
- $M \approx 2ka \rightarrow M = 27$

Sources:

- Plane waves
- $V \approx 2ka \rightarrow V = 27$
- Amplitude $A = 1$
- Frequency: 300 MHz $(\lambda = 1)$

Object:

- Square cylinder of side $\frac{\lambda}{3} = 0.33$
- $\varepsilon_r \in \{1.5, 2.0, 2.5, 3.0\}$
- $\sigma = 0$ [S/m]

BCS parameters:

- Initial estimate of the noise: $n_0 = 1.0 \times 10^{-3}$
- Convergenze parameter: $\tau = 1.0 \times 10^{-8}$

RESULTS: $\varepsilon_r = 1.5$

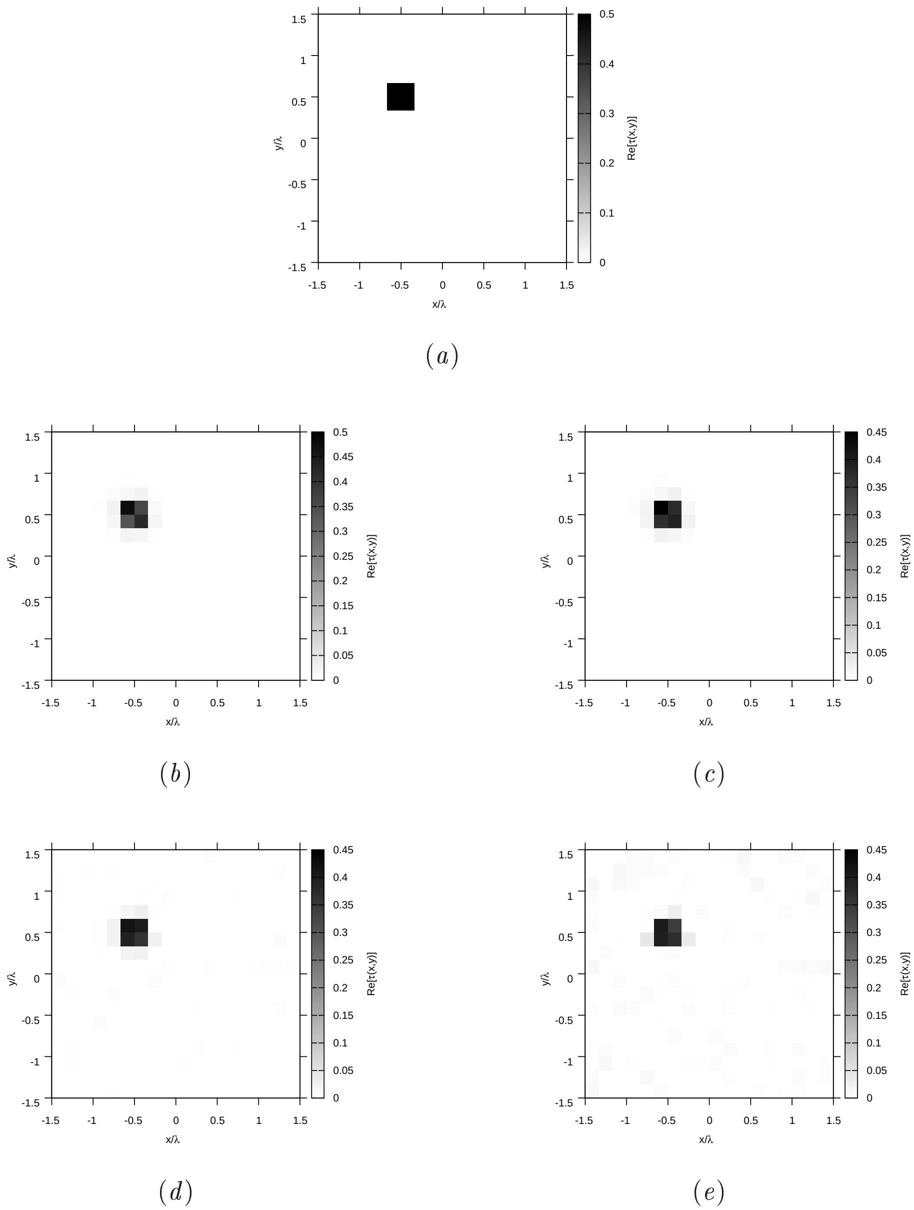

Figure 9. Actual object (a) and BCS reconstructed object for (b) Noiseless case, (c) $SNR = 20$ [dB] , (d) $SNR = 10$ [dB] , (e) $SNR = 5$ [dB].

Observations:

Ricostruzioni buone per i casi Noiseless, $SNR = 20\,dB$ e $SNR = 10\,dB$; compare del rumore di fondo per il caso $SNR = 5\,dB$.

RESULTS: $\varepsilon_r = 2.0$

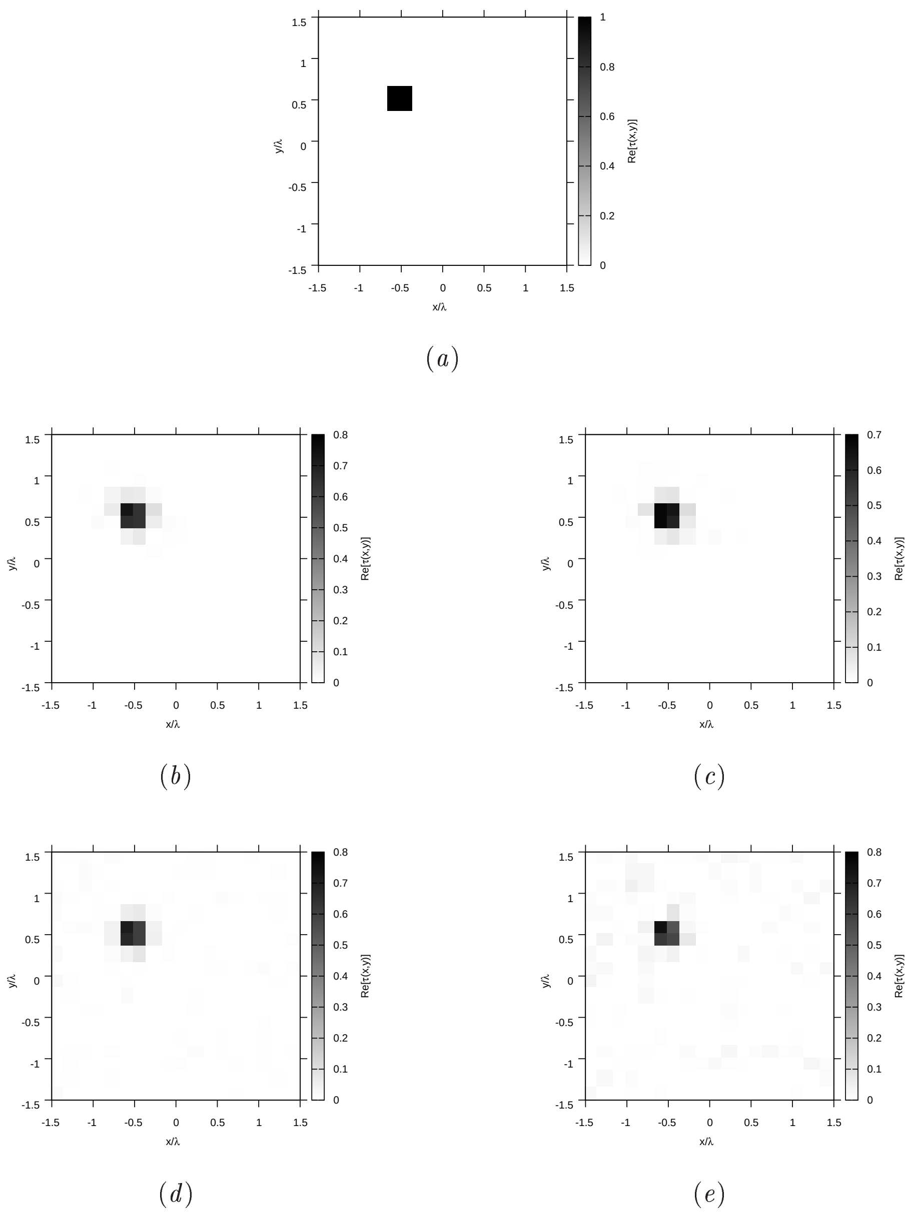

Figure 10. Actual object (a) and BCS reconstructed object for (b) Noiseless case, (c) $SNR = 20$ [dB] , (d) $SNR = 10$ [dB] , (e) $SNR = 5$ [dB].

Observations:

Ricostruzioni abbastanza buone per i casi Noiseless, $SNR = 20\,dB$ e $SNR = 10\,dB$; compare del rumore di fondo per il caso $SNR = 5\,dB$.

RESULTS: $\varepsilon_r = 2.5$

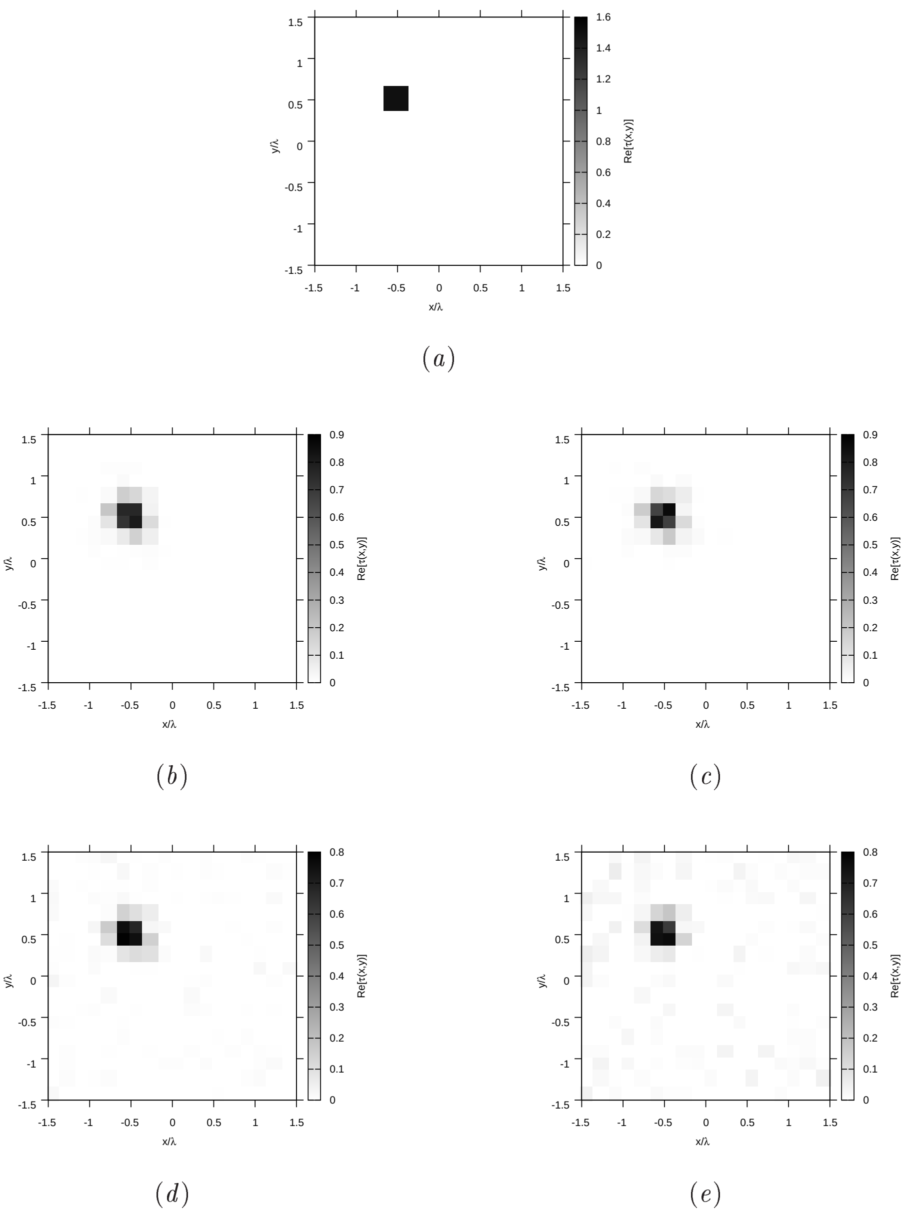

Figure 11. Actual object (a) and BCS reconstructed object for (b) Noiseless case, (c) $SNR = 20$ [dB] , (d) $SNR = 10$ [dB] , (e) $SNR = 5$ [dB].

Observations:

Ricostruzioni sempre più degradate: approssimazione di Born non più applicabile.

RESULTS: $\varepsilon_r = 3.0$

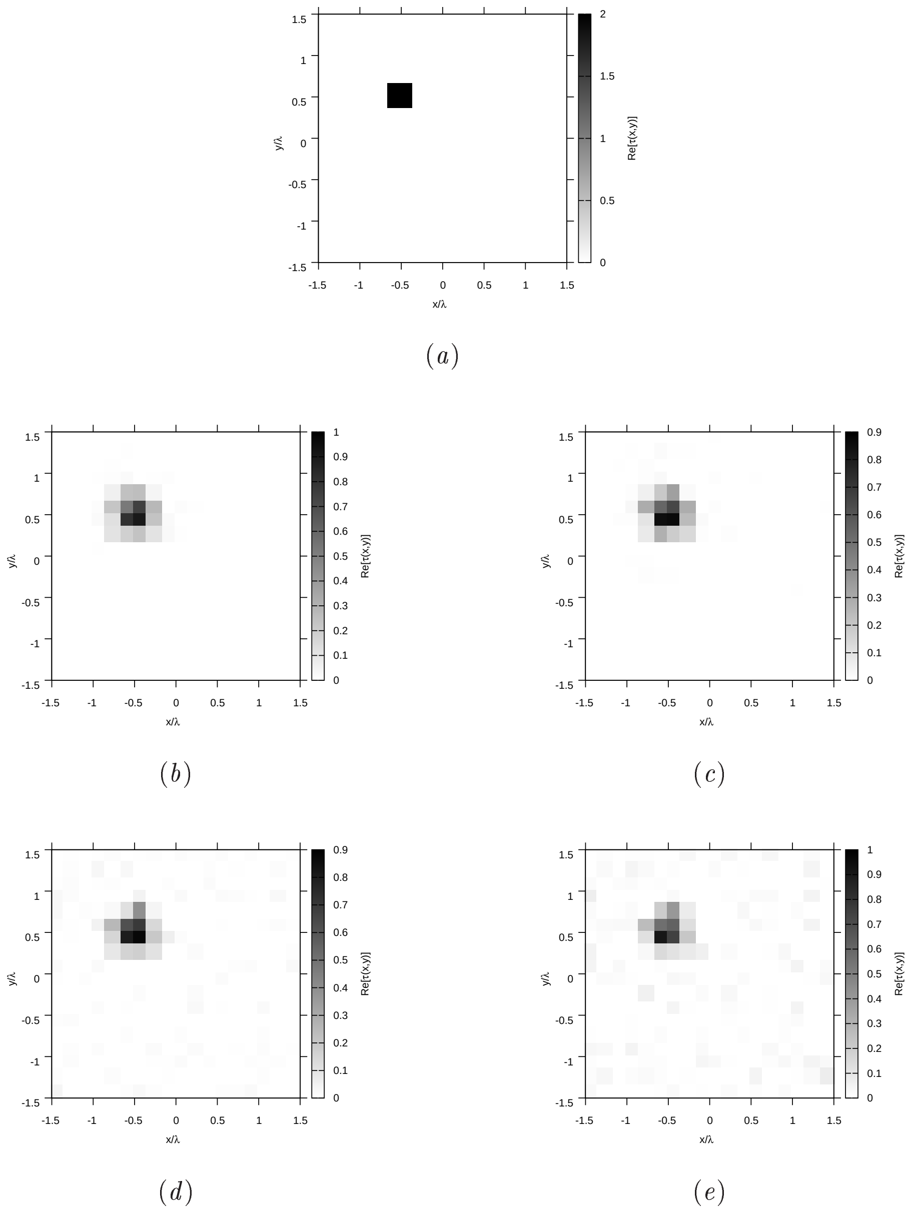

Figure 12. Actual object (a) and BCS reconstructed object for (b) Noiseless case, (c) $SNR = 20$ [dB] , (d) $SNR = 10$ [dB] , (e) $SNR = 5$ [dB].

Observations:

Ricostruzioni sempre più degradate: approssimazione di Born non più applicabile.

RESULTS: Error Figures

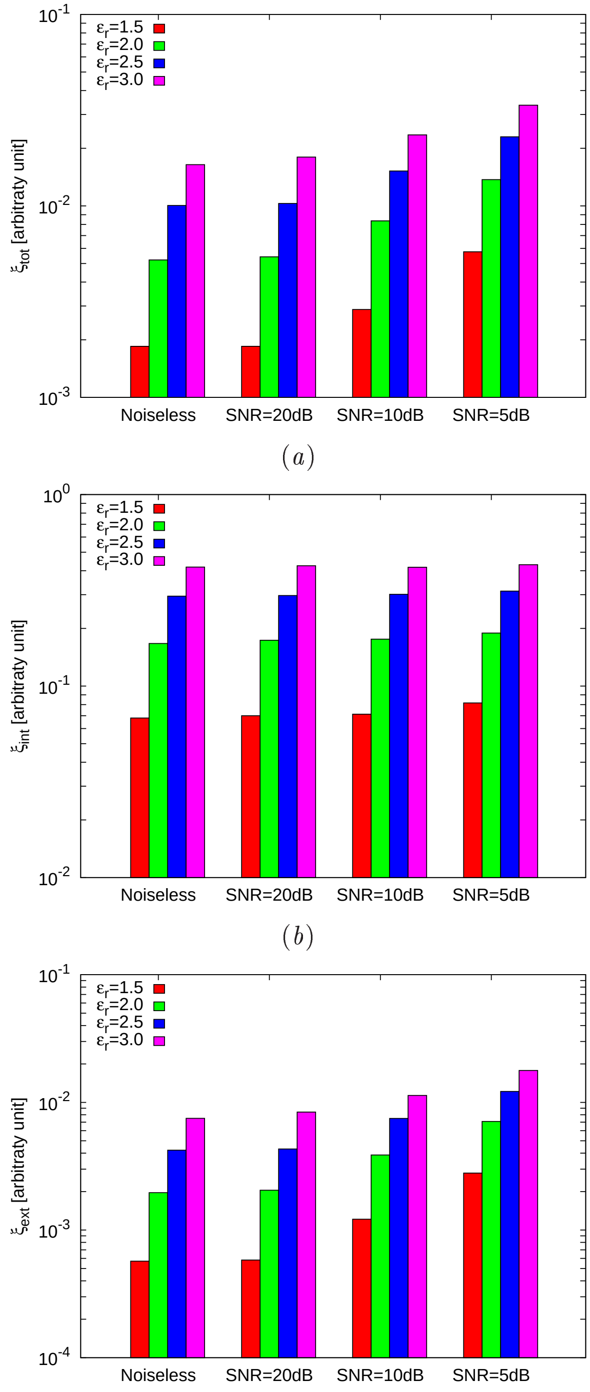

Figure 13. Behaviour of error figures as a function of ε_r, for different SNR values: (a) total error ξ_{tot}, (b) internal error ξ_{int}, (c) external error ξ_{ext}.

RESULTS: Error Figures

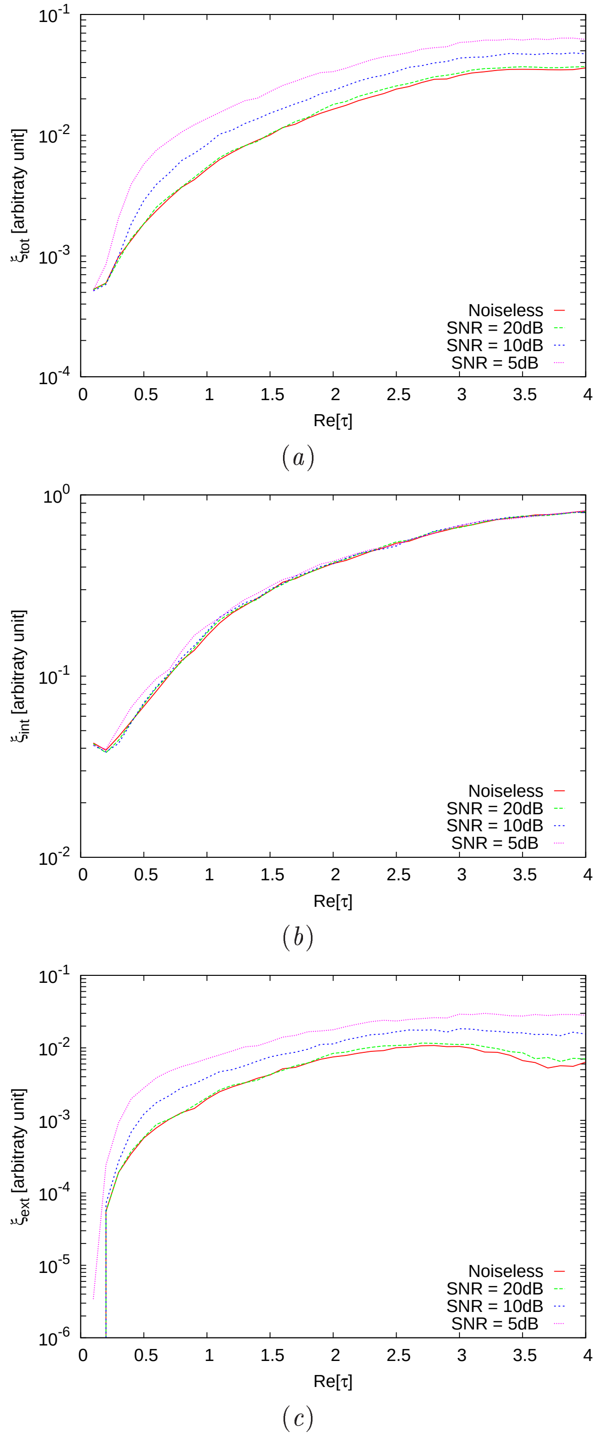

Figure 14. Behaviour of error figures as a function of ε_r, for different SNR values: (a) total error ξ_{tot}, (b) internal error ξ_{int}, (c) external error ξ_{ext}.

Internal Scattered Field Analysis

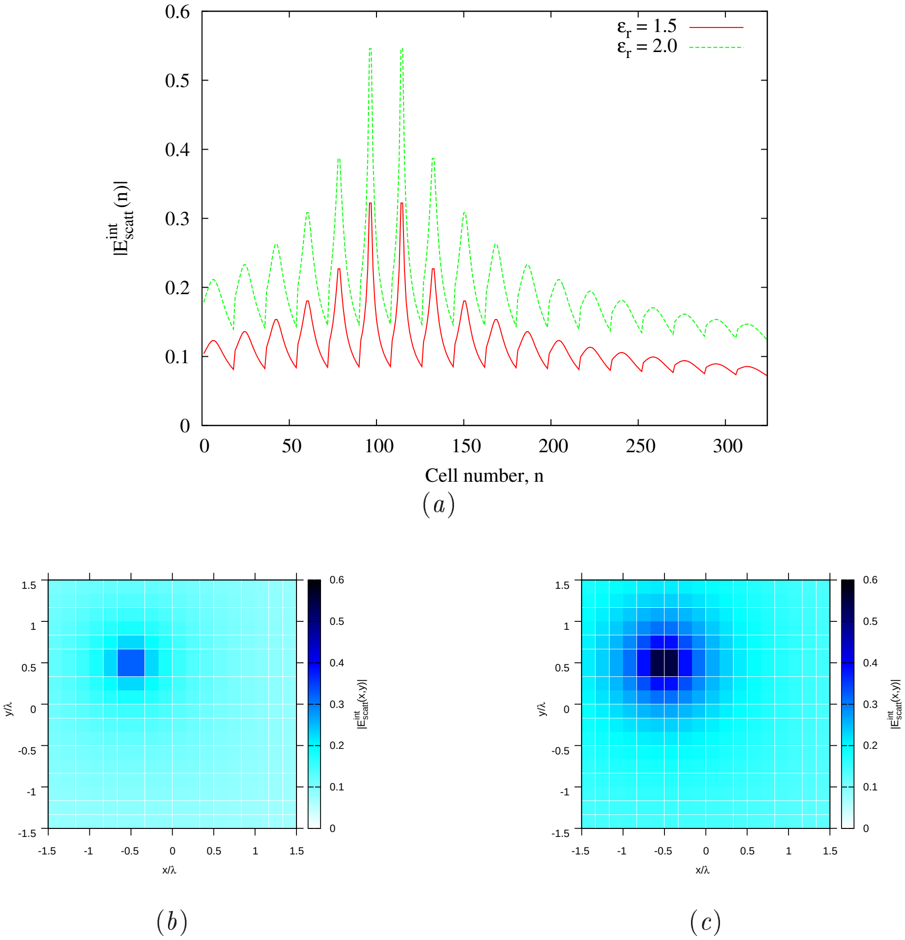

Figure 15.(a) Average of the absolute value of the scattered field inside the investigation domain for different values of ε_r : (b) $\varepsilon_r = 1.5$, (c) $\varepsilon_r = 2.0$.

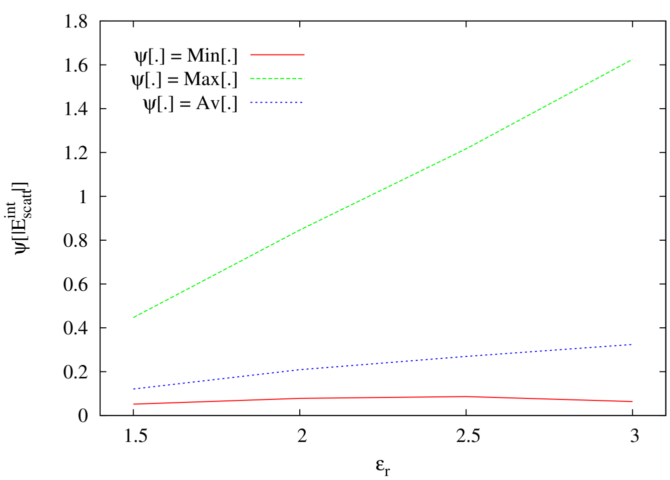

(a)

Figure 16.(a) Internal Scattered Field statistical analysis.

Observations:

Le prestazioni della tecnica si possono considerare buone fino a $\varepsilon_r = 2.0$, ossia, osservando Fig.16.(a), anche in questo caso come nel TEST CASE precedentemente analizzato (singolo quadrato, dimensioni $\lambda/6$), fino a quando $\frac{E_{tot}^{int} - E_{inc}^{int}}{E_{inc}^{int}} < 0.2$.

References

[1] E. J. Candes and M. B. Wakin, "An introduction to compressive sampling", *IEEE Signal Processing Magazine*, vol. 25, no. 2, pp. 21-30, March 2008.

[2] S. Ji, Y. Xue, and L. Carin, "Bayesian compressive sampling", *IEEE Trans. on Signal Processing*, vol. 56, no. 6, pp. 2346-2356, June 2008.

[3] R. F. Harrington, *Field computation by moment methods*, New York: IEEE Press, 1993.

[4] J. H. Richmond, "Scattering by a dielectric cylinder of arbitrary cross shape", *IEEE Trans. Antennas Propagat.*, vol. AP-13, no. 3, pp. 334-341, May 1965.

[5] M. Slaney, A. C. Kak, and L. E. Larsen, "Limitations of imaging with first-order diffraction tomography", *IEEE Trans. on Microwave Theory and Techniques*, vol. MTT-32, no. 8, pp. 860-874, Aug. 1984.

[6] L. Poli, G. Oliveri, and A. Massa, "Imaging sparse metallic cylinders through a Local Shape Function Bayesian Compressive Sensing approach," Journal of Optical Society of America A, vol. 30, no. 6, pp. 1261-1272, 2013.

[7] F. Viani, L. Poli, G. Oliveri, F. Robol, and A. Massa, "Sparse scatterers imaging through approximated multitask compressive sensing strategies," Microwave Opt. Technol. Lett., vol. 55, no. 7, pp. 1553-1558, Jul. 2013.

[8] L. Poli, G. Oliveri, P. Rocca, and A. Massa, "Bayesian compressive sensing approaches for the reconstruction of two-dimensional sparse scatterers under TE illumination," IEEE Trans. Geosci. Remote Sensing, vol. 51, no. 5, pp. 2920-2936, May. 2013.

[9] L. Poli, G. Oliveri, and A. Massa, "Microwave imaging within the first-order Born approximation by means of the contrast-field Bayesian compressive sensing," IEEE Trans. Antennas Propag., vol. 60, no. 6, pp. 2865-2879, Jun. 2012.

[10] G. Oliveri, P. Rocca, and A. Massa, "A bayesian compressive sampling-based inversion for imaging sparse scatterers," IEEE Trans. Geosci. Remote Sensing, vol. 49, no. 10, pp. 3993-4006, Oct. 2011.

[11] G. Oliveri, L. Poli, P. Rocca, and A. Massa, "Bayesian compressive optical imaging within the Rytov approximation," Optics Letters, vol. 37, no. 10, pp. 1760-1762, 2012.

[12] L. Poli, G. Oliveri, F. Viani, and A. Massa, "âMT-BCS-based microwave imaging approach through minimum-norm current expansion," IEEE Trans. Antennas Propag., in press. doi:10.1109/TAP.2013.2265254

[13] S. C. Hagness, E. C. Fear, and A. Massa, "Guest Editorial: Special Cluster on Microwave Medical Imaging", IEEE Antennas Wireless Propag. Lett., vol. 11, pp. 1592-1597, 2012.

[14] G. Oliveri, Y. Zhong, X. Chen, and A. Massa, "Multi-resolution subspace-based optimization method for inverse scattering," Journal of Optical Society of America A, vol. 28, no. 10, pp. 2057-2069, Oct. 2011.

[15] A. Randazzo, G. Oliveri, A. Massa, and M. Pastorino, "Electromagnetic inversion with the multiscaling inexact-Newton method - Experimental validation," Microwave Opt. Technol. Lett., vol. 53, no. 12, pp. 2834-2838, Dec. 2011.

[16] G. Oliveri, L. Lizzi, M. Pastorino, and A. Massa, "A nested multi-scaling inexact-Newton iterative approach for microwave imaging," IEEE Trans. Antennas Propag., vol. 60, no. 2, pp. 971-983, Feb. 2012.

[17] G. Oliveri, A. Randazzo, M. Pastorino, and A. Massa, "Electromagnetic imaging within the contrast-source formulation by means of the multiscaling inexact Newton method," Journal of Optical Society of America A, vol. 29, no. 6, pp. 945-958, 2012.

[18] M. Benedetti, D. Lesselier, M. Lambert, and A. Massa, "Multiple shapes reconstruction by means of multi-region level sets," IEEE Trans. Geosci. Remote Sensing, vol. 48, no. 5, pp. 2330-2342, May 2010.

[19] M. Benedetti, D. Lesselier, M. Lambert, and A. Massa, "A multi-resolution technique based on shape optimization for the reconstruction of homogeneous dielectric objects," Inverse Problems, vol. 25, no. 1, pp. 1-26, Jan. 2009.

[20] M. Donelli, D. Franceschini, P. Rocca, and A. Massa, "Three-dimensional microwave imaging problems solved through an efficient multi-scaling particle swarm optimization," IEEE Trans. Geosci. Remote Sensing, vol. 47, no. 5, pp. 1467-1481, May 2009.

[21] M. Benedetti, G. Franceschini, R. Azaro, and A. Massa, "A numerical assessment of the reconstruction effectiveness of the integrated GA-based multicrack strategy," IEEE Antennas Wireless Propag. Lett., vol. 6, pp. 271-274, 2007.

[22] P. Rocca, M. Carlin, G. Oliveri, and A. Massa, "Interval analysis as applied to inverse scattering," IEEE International Symposium on Antennas Propag. (APS/URSI 2013), Chicago, Illinois, USA, Jul. 8-14, 2012.

[23] L. Manica, P. Rocca, M. Salucci, M. Carlin, and A. Massa, "Scattering data inversion through interval analysis under Rytov approximation," 7th European Conference on Antennas Propag. (EuCAP 2013), Gothenburg, Sweden, Apr. 8-12, 2013.

[24] P. Rocca, M. Carlin, and A. Massa, "Imaging weak scatterers by means of an innovative inverse scattering technique based on the interval analysis," 6th European Conference on Antennas Propag. (EuCAP 2012), Prague, Czech Republic, Mar. 26-30, 2012.

[25] G. Oliveri and A. Massa, "Bayesian compressive sampling for pattern synthesis with maximally sparse non-uniform linear arrays," IEEE Trans. Antennas Propag., vol. 59, no. 2, pp. 467-481, Feb. 2011.

[26] G. Oliveri, M. Carlin, and A. Massa, "Complex-weight sparse linear array synthesis by Bayesian Compressive Sampling," IEEE Trans. Antennas Propag., vol. 60, no. 5, pp. 2309-2326, May 2012.

[27] G. Oliveri, P. Rocca, and A. Massa, "Reliable Diagnosis of Large Linear Arrays - A Bayesian Compressive Sensing Approach," IEEE Trans. Antennas Propag., vol. 60, no. 10, pp. 4627-4636, Oct. 2012.

[28] F. Viani, G. Oliveri, and A. Massa, "Compressive sensing pattern matching techniques for synthesizing planar sparse arrays" IEEE Trans. Antennas Propag., in press. doi:10.1109/TAP.2013.2267195

[29] M. Carlin, P. Rocca, G. Oliveri, F. Viani, and A. Massa, "Directions-of-Arrival Estimation through Bayesian Compressive Sensing strategies," IEEE Trans. Antennas Propag., in press.

[30] M. Carlin, P. Rocca, "A Bayesian compressive sensing strategy for direction-of-arrival estimation," 6th European Conference on Antennas Propag. (EuCAP 2012), Prague, Czech Republic, pp. 1508-1509, 26-30 Mar. 2012.

[31] M. Carlin, P. Rocca, G. Oliveri, and A. Massa, "Bayesian compressive sensing as applied to directions-of-arrival estimation in planar arrays", Journal of Electrical and Computer Engineering, Special Issue on "Advances in Radar Technologies", in press.